J. Fluid Mech. (1992), *vol.* 234, *pp.* 191–217
Printed in Great Britain

Aspect ratio and end plate effects on vortex shedding from a circular cylinder

By S. SZEPESSY[1] AND P. W. BEARMAN[2]

[1] Department of Thermo and Fluid Dynamics, Chalmers University of Technology, 41296 Gothenburg, Sweden

[2] Department of Aeronautics, Imperial College of Science Technology and Medicine, London SW7 2BY, UK

(Received 16 November 1990 and in revised form 28 June 1991)

Aspect ratio effects on the vortex shedding flow from a circular cylinder have been studied by using moveable end plates. Experiments were carried out to measure fluctuating forces, shedding frequency and spanwise correlation whilst varying end plate separation and Reynolds number. The aspect ratio (0.25–12) was found to have a most striking effect on the fluctuating lift. Within a certain range of Reynolds number an increase of the sectional fluctuating lift was obtained for reduced aspect ratio, and showed a maximum for an aspect ratio of 1, where the fluctuating lift could be almost twice the value for very large aspect ratios. This increase of the lift amplitude was found to be accompanied by enhanced spanwise correlation of the flow. The measurements were carried out over the Reynolds number range $8 \times 10^3 < Re < 1.4 \times 10^5$. The strong increase in fluctuating lift with small aspect ratio did not occur at the lower and upper boundaries of this range. In the lower Reynolds number range ($Re < 2 \times 10^4$) the trend could be reversed, i.e. the fluctuating lift decreased with decreasing aspect ratio. Also, with small aspect ratio, a shedding breakdown was found in the upper Reynolds number range ($Re = 1.3 \times 10^5$). The main three-dimensional feature observed was a spanwise variation in the phase of vortex shedding, accompanied by amplitude modulation in the lift signal. However, the level of three-dimensionality can be reduced by using a small aspect ratio. Three-dimensional vortex shedding features are discussed and comparison of the results with those from both two-dimensional numerical simulations and other experiments using large aspect ratios are presented.

1. Introduction

Numerous investigations of various aspects of the flow around a circular cylinder in crossflow have been reported, but only a few, and mainly the more recent ones, focus attention on three-dimensional aspects. Three-dimensional flow on a fixed circular cylinder can be influenced by a number of effects. A case of strong three-dimensional flow is a cylinder with a free end, but the flow can be modified by end plates or end walls limiting the aspect ratio, i.e. the ratio of cylinder span length to cylinder diameter L/D. The latter cases produce three-dimensional effects by interaction with the wall boundary layer, which also affects the flow behind a cylinder by limiting crossflow along the cylinder axis near the end plate or end wall. This crossflow may be the result of an instability of the vortex filaments which leads to slanted shedding or shedding in cells, either in an organized or random pattern, depending on the Reynolds number Re. The present results are obtained from a

circular cylinder with moveable end plates and measurements are presented of changes in the vortex shedding parameters with aspect ratio.

There is an increasing interest in three-dimensional flow effects on nominal two-dimensional bodies. Partly, this increasing awareness had arisen because two-dimensional numerical simulations fail to predict accurately some of the vortex shedding parameters of circular cylinder wakes. However, at low Reynolds number, where the flow observed in experiments is fully laminar, two-dimensional numerical direct simulations by Braza, Chassaing & Ha Minh (1986, 1990) have successfully predicted pressure and wake formation size in the steady recirculating wake Reynolds number range and also in the lower vortex shedding range. Braza *et al.*'s calculations cover a substantial part of the vortex shedding range, up to $Re = 1 \times 10^4$. They found it impossible to predict a critical Reynolds number for the onset of vortex shedding that compares well with experiments, i.e. around $Re = 40$. This shortcoming is attributed to the numerical model's lack of natural disturbances, which may have to be modelled in three dimensions for a fully adequate representation. Experiments in the steady wake regime by Shair *et al.* (1963) and Nishioka & Sato (1974) have shown that the onset of vortex shedding does not occur at a universal Reynolds number but is strongly dependent on aspect ratio. Their work is further discussed later in this section. After the onset of vortex shedding, three-dimensionality is found in the laminar vortex street range unless the end conditions are very carefully controlled, as discussed by Williamson (1989) and Eisenlohr & Eckelmann (1989). At higher Reynolds number, which is the subject of this paper, three-dimensionality is perhaps triggered by the higher level of disturbances introduced by turbulence. Some parameters, like Strouhal number and the coefficient of mean drag have been well captured in Braza *et al.*'s calculations. However, these features seem to be not as sensitive to disturbances as the fluctuating lift, which according to the present survey will require a three-dimensional model for adequate representation. It is difficult to say at which Reynolds number the deviation between a two-dimensional numerical model and experiments starts, since the present work and Braza *et al.*'s only overlap at the limits of our respective Reynolds number ranges, i.e. $Re = 10^4$. To measure the fluctuating lift for lower Reynolds numbers is difficult. An attempt was made by Tanida, Okajima & Watanabe (1973) using strain gauges on small cylinders in both oil and water channels at Reynolds numbers of 150 and 1000. Although the accuracy of their measurements is not given, the results imply that the fluctuating lift coefficient grows much slower with increasing Reynolds number than predicted by a two-dimensional numerical simulation. Measurements by Tadrist *et al.* (1990), using aspect ratio $L/D = 12.5$–30, show that there is a sharp reduction in the fluctuating lift for Reynolds numbers below 10^4, down to the lower boundary of their measured range ($Re = 3000$).

The flow at higher Reynolds numbers, as has been investigated in this report, is very difficult to calculate numerically at present owing to the need to resolve thin shear layers and turbulence. In experiments end effects can be recognized up to at least 30 body diameters from a boundary with a poor end plate design, also the vortices shed are not two-dimensional but exhibit spanwise variations in strength and position. Both from a fundamental and a practical point of view, three-dimensional effects are important and should properly be taken into account. Tubes and pipes in crossflow, even if they are very long, will experience three-dimensional effects near the points of attachment. In an engineering application a number of important effects may result from any three-dimensional behaviour. Both mean and

fluctuating forces may change and this will be important for the design of structures. For example, the combined effects of changes to the forces and heat transfer experienced by tubes in a heat exchanger have an important influence on performance.

Despite increased awareness of these effects the understanding of the physical process causing them is by no means complete. It has been shown by Humphreys (1966) that the surface flow around a cylinder divides into stationary cells along the cylinder span at the critical Reynolds number ($Re = 3 \times 10^5$). In the subcritical range there are no steady cellular structures present and when Humphrey's reduced the Reynolds number slightly below the critical value, he observed that the cells started to move along the surface. At present detailed knowledge about the origin and effect of spanwise vortex shedding structures is still lacking. However, introduction of three-dimensional flow by free end boundaries has been studied somewhat further and one of the first to report on three-dimensional effects on circular cylinder flow with free ends was Wieselberger (1923) who reported decreased mean drag for cylinders of small length. He used a set of cylinders of different lengths with L/D ranging from 1 to 280. He suggested that the reduced drag for cylinders of small length was due to crossflow limiting the pressure difference between the free stream and the near-wake region. This problem has been studied in more detail recently by Zdravkovich *et al.* (1989) (two free ends) and (one free end) by Kareem, Cheng & Lu (1989), Baban, So & Ötügen (1989), Sin & So (1987) and Farivar (1981). The common trend is that regular, alternating vortex shedding diminishes towards the free end of the cylinder. Interestingly, despite irregular vortex shedding, the level of fluctuating pressure near the free end exceeds that of the regular shedding fluctuations closer to the base of the cylinder. Farivar (1981) found that the fluctuating pressure peaked at $y/L = 0.95$, with y measured from the base of the cylinder.

On a high aspect ratio cylinder there are unsteady pressure gradients along the span, as evidenced by vortex shedding not being in phase along the span. At the cylinder the free shear layers do not roll up in a two-dimensional manner and this leads to pressure differences causing crossflow in the near wake. Near an end plate this unsteady crossflow is suppressed and this may lead to an enhancement in vortex shedding uniformity, i.e. the opposite effect to a free end. The present experiments show that the end plates do have this effect, and it is also shown over how long a distance this influence stretches.

Work emphasizing the importance of end plates has been reported by several researchers. Keefe (1961) measured increased fluctuating lift force on a circular cylinder of small aspect ratio ($L/D = 3$) using strain gauges connected to a short spanwise active length. These results gave a considerably larger fluctuating lift than those obtained at larger aspect ratios. The changes in fluctuating drag were very small and appeared to be within the error margins of the measurement system. Owing to the length of the force cell, Keefe could not study very small aspect ratio flows. Cowdrey (1962) investigated the effect of using end plates on the drag of a square bar. A strong increase in the drag was recorded when using end plates. The length of the end plates was chosen such that there was no flow around their trailing edges. Wool tufts were used to determine flow direction around the edge. The static pressure in the wake increases rather slowly downstream of a bluff body and it may require an end plate several body diameters long before the crossflow is suppressed. If the distance to the trailing edge of the end plate is shorter than this there may be a disturbance strong enough to change vortex shedding. Cowdrey came to the conclusion that if end plates are to be effective then they have to be carefully

designed. In later work, Stansby (1974) and Kubo, Miyazaki & Kato (1989) came to similar conclusions.

Bearman (1965) reported that on a two-dimensional body with a blunt trailing edge the base pressure could be made more nearly uniform across the span by using end plates. Stansby (1974) reached the same conclusion for a circular cylinder flow. Stansby was concerned particularly with end plate size and argues similarly to Cowdrey that there is a minimum end plate size required to give closely two-dimensional wake flow. He carefully chose the leading and trailing edge distances to the cylinder axis. These earlier investigations have given some insight into end plate effects but a full understanding of the influence of end plates is still lacking and hence it is in this context the present paper hopes to make a contribution. There are still problems in explaining both how the three-dimensional flow created by the forward side of the plate interacts with vortex shedding and how significant this effect is, as well as determining the rear side effect on shedding which directly influences the near wake.

For completeness, end plate and aspect ratio effects at lower Reynolds number will also be briefly reviewed here, though it is clear that comparisons with the present Reynolds number range should be made with caution. Within the range of the present experiments the Reynolds number dependence is striking and it is shown that a breakdown in vortex shedding occurs at a critical Reynolds number that depends on aspect ratio. At low Reynolds numbers, circular cylinder flow undergoes a change whereby the flow in the wake become unstable leading to alternate vortex shedding. The onset of this vortex shedding is dependent on the disturbance level in the flow and the proximity of the flow boundaries which appear to dampen out perturbations. The effectiveness of using confining walls limiting the aspect ratio (width/diameter, L/D), and height/diameter, H/D, to suppress the onset of vortex shedding has been pointed out by Shair *et al.* (1963). They showed that the onset of vortex shedding could be delayed by using confining walls and changing L/D over the range from 16 to 4 and H/D from 20 to 5. The critical Reynolds number could then be increased from 50 to 130. It should also be noted that for the largest aspect ratio they used they did not find a critical Reynolds number around 40 as obtained in other experiments for long spans. However, Williamson (1989) recently reported a critical Reynolds number of 49 for long span cylinders. Nishioka & Sato (1974) performed experiments using moveable end plates to change the aspect ratio. They also obtained enhanced stabilization of the wake, using an aspect ratio of 6.5. The onset of the vortex shedding range was delayed to a Reynolds number of 150. Limiting values of $Re = 48$ were found for end plate separations larger than $50D$.

For similar Reynolds numbers Slaouti & Gerrard (1981) studied the three-dimensionality of the wake of a cylinder towed through water. They studied the effect of a free end, an end plate and a free water surface on the shedding pattern of the wake by means of flow visualization. In common with a number of other workers they observed slantwise shedding in the laminar shedding regime. They suggested that slantwise shedding was not an intrinsic feature of the wake but a consequence of the end configuration used. Gerich & Eckelmann (1982) and Gerich (1986) further studied the end plate influence by measuring the shedding frequency along the cylinder span and found reduced Strouhal numbers in the regions close to the end plates. Several investigators, including Williamson (1989) and König, Eisenlohr & Eckelmann (1990), have shown since that in the laminar vortex street range the Strouhal number measured at the centre span is influenced by end boundary conditions for very long spans. Williamson discussed how low-frequency vortex

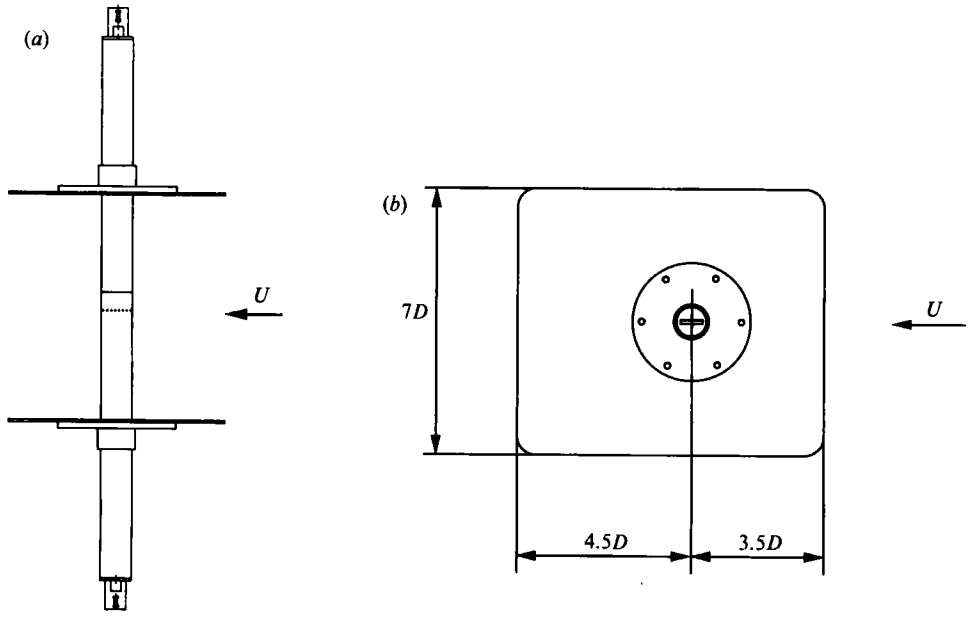

FIGURE 1. (*a*) Cylinder with end plates. (*b*) Side view of an end plate.

shedding cells at the end plates interface with higher frequency shedding cells in the midspan region resulting in the previously observed oblique vortex shedding. Williamson showed that by yawing the end plates, a constant shedding frequency could be achieved along the whole span. König *et al.* (1990) achieved a constant spanwise shedding frequency by using larger diameter end cylinders. Extending the Reynolds number range beyond the laminar shedding mode, Gerich (1986) performed measurements in the lower subcritical turbulent vortex shedding regime, up to a Reynolds number of 2600. In the so called 'end plate affected region' strong modulation of the velocity signals associated with vortex shedding was observed, similar to that seen by Keefe (1961) and in the present paper for much higher Reynolds number.

2. Experimental arrangement

The experiments were conducted in a low-speed wind tunnel at the Department of Aeronautics, Imperial College, London. The tunnel is of closed circuit design with the working section measuring (in m) 0.91 high × 0.91 wide × 5.49 long. The turbulence level is less than 0.05% and the velocity variation across the section is less than $\pm\frac{1}{2}\%$ outside the wall boundary layer. The circular cylinder used was 6 cm in diameter and made from Perspex tube. It was positioned horizontally at midheight 1.3 m downstream of the start of the working section. The cylinder was fitted with moveable end plates which allowed aspect ratio changes without changing blockage, which remained constant at 7.7%. The end plates were designed following recommendations by Stansby (1974). They were rectangular shaped plates 8*D* long by 7*D* wide and the distance between the cylinder axis and the leading edge was 3.5*D*. Figure 1 (*a*) shows the cylinder with the end plates fitted and figure 1 (*b*) shows a side view of an end plate. Both the cylinder and the end plates were made of Perspex.

The lift and drag forces were obtained by using a spatial pneumatic pressure

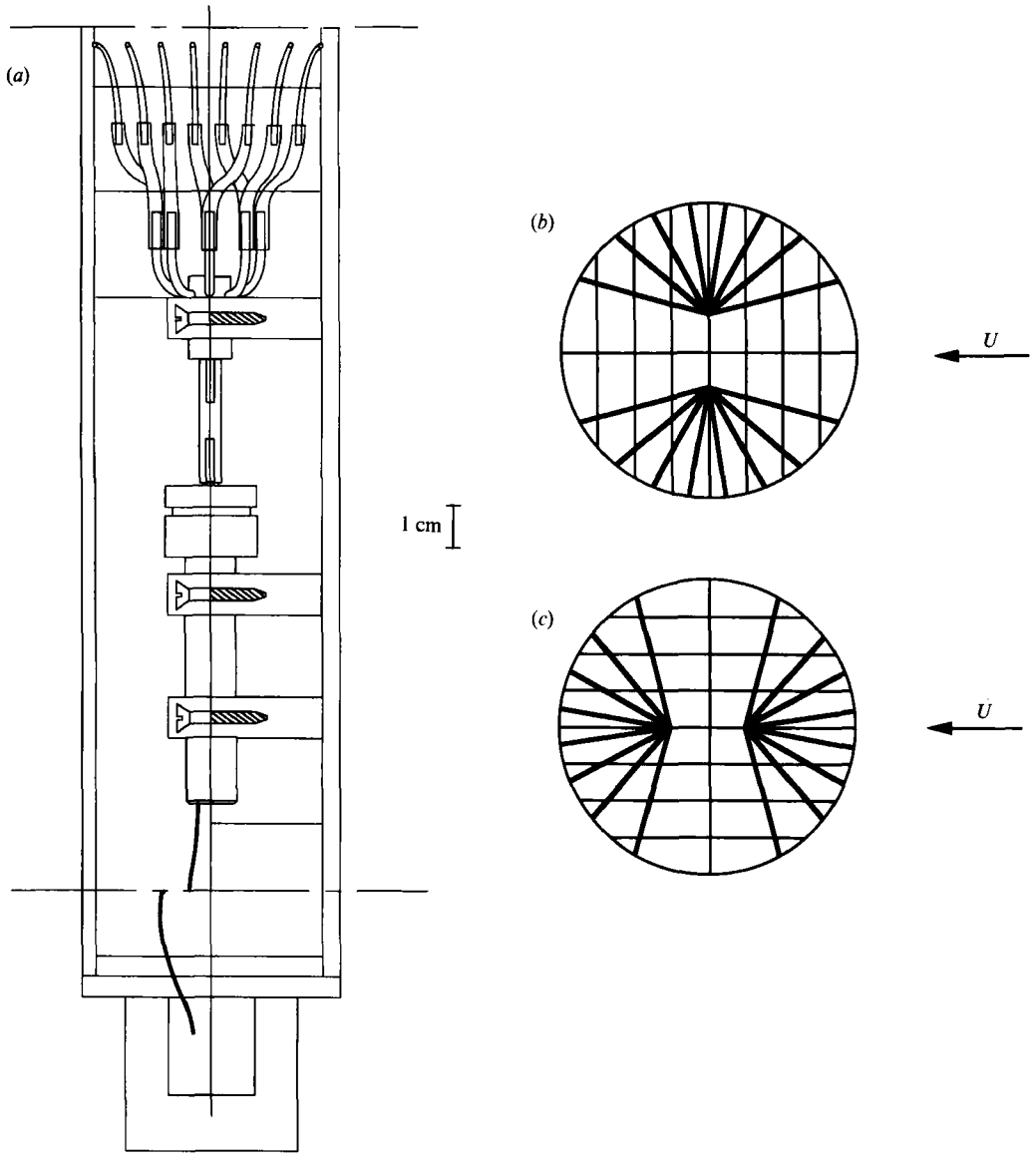

FIGURE 2. (a) The spatial pressure averaging system with the transducers mounted inside the cylinder. (b) Positioning of the pressure tappings for fluctuating lift measurements. (c) Positioning of the pressure tappings for drag measurements.

averaging technique first used by Surry & Stathopoulos (1977). The averaging device shown in figure 2(a) consists of eight pressure tappings suitably positioned in one plane around a semicircle, all connected to a manifold with one output. This output is connected to a high sensitivity differential Setra 237 pressure transducer with a range of ± 0.1 p.s.i. There are two identical arrangements for simultaneous measurements on both halves of the cylinder cross-section. The outputs of the pressure transducers were taken to a microcomputer via analog to digital converters. By subtracting the two pressure transducer outputs, sectional time-dependent forces could be evaluated. By rotating the cylinder and appropriately positioning it, lift

as in figure 2(*b*) or drag as in figure 2(*c*), could be obtained. This type of force measurement involves some approximations, which subsequently have been studied in detail and shown not to introduce serious errors. A brief outline of likely errors arising with this method will be given below. The first approximation involves the integration of pressure along the surface with only eight discrete increments per semicircle. A satisfactory agreement for mean forces was obtained with data from a pressure distribution around the cylinder using curve fitting and 1° increment integration with Simpson's extended rule. The mean lift force on a semicircle (upper or lower) obtained from the manifold gave $\overline{c_L} = -1.10$, while the Simpson integration gave

$$\overline{c_L} = \frac{1}{2}\int_0^{\pi} c_p \sin\phi \, \mathrm{d}\phi = -1.097.$$

This excellent agreement was not reproduced in the drag direction where the manifold gave $\overline{c_{D\text{front}}} = 0.06$, $\overline{c_{D\text{rear}}} = 1.36$ and hence a total drag of $\overline{c_D} = 1.42$, whilst the Simpson integration gave $\overline{c_{D\text{front}}} = -0.06$, $\overline{c_{D\text{rear}}} = 1.37$ and an overall drag of $\overline{c_D} = 1.31$. The error arising on the front is not due to poor spatial resolution of the pressure tappings, as a sum of the eight corresponding pressures from the pressure distribution gave $\overline{c_{D\text{from}}} = -0.04$, which agrees well with the fine Simpson integration value of $\overline{c_{D\text{front}}} = -0.06$. Instead, this is an error caused by the averaging manifold itself. It is quite plausible that there is a small leakage flow from the taps near the stagnation point through the averaging chamber back to the external flow via the taps at the low-pressure region. Immediately one can question whether this small leakage flow affects the external flow. As the pressure distribution did not change whilst recording pressure from an individual pressure tap with firstly having the force measuring taps sealed and secondly having them connected to the manifolds for force measurements, it was assessed that the pressure averaging technique does not affect the external vortex shedding flow.

The above values have not been corrected for blockage. Allen & Vincenti's (1944) formula reduces the overall drag coefficient to $\overline{c_D} = 1.32$ from the manifold and to $\overline{c_D} = 1.24$ for the Simpson integration which agrees well with values found in the literature at the same Reynolds number. The error in the drag measurements is not of major concern as this investigation aims at studying the vortex shedding process under various aspect ratio effects which is best seen as changes in fluctuating lift. Also, the fluctuating lift is of more practical importance since it is almost an order of magnitude larger than the fluctuating drag. Nevertheless, the estimation of fluctuating drag and the trends in changes of mean drag are believed to be fairly accurate since the front face, where the error is produced, contributes very little to the fluctuating drag, and also the changes in mean drag are essentially due to a change in base pressure.

The next feature of importance is the dynamic response of the pressure tubing system, the averaging manifold and the transducer itself. The transducer is of high performance and according to the manufacturer gives a linear output up to several hundred Hz. The tubing system connected to the averaging manifold was calibrated using a closed chamber of circular cross-section where one end wall houses a loudspeaker producing harmonic pressure fluctuations controlled by a sine wave generator. The other end consists of a flat wall where a flush surface pressure transducer and several pressure tappings were mounted. Comparing the output from the flush surface transducer and the averaging manifold makes it possible to determine the upper frequency at which the averaging manifold could be used. The

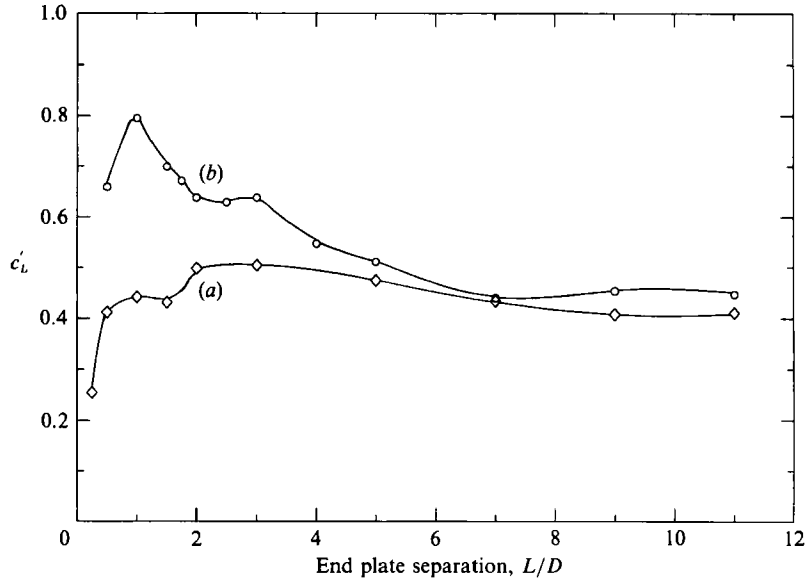

FIGURE 3. Fluctuating lift *vs.* end plate separation: (*a*) $Re = 1.6 \times 10^4$; (*b*) $Re = 4.3 \times 10^4$.

calibration showed that the pressure averaging system had a gain near unity up to about 300 Hz, whilst the highest shedding frequency throughout the survey was 110 Hz. The first natural harmonic of the tubing system was at 600 Hz. The signals were always low-pass filtered during the measurements. A phase lag between the flush surface transducer and manifold was detected below the filter cutoff frequency but this was similar for both manifolds and did not affect the measurements of fluctuating force. For cross-correlation and frequency analysis, in addition to a stationary pressure tap a standard hot-wire anemometer (TSI) with a normal probe was used and could be moved along all three axes with a traversing system attached to the tunnel roof.

3. Fluctuating lift

3.1. *Coefficient of fluctuating lift vs. end plate separation*

To illustrate the most basic and typical aspect ratio effects on vortex shedding, the coefficient of fluctuating lift (c_L') is presented as a function of end plate separation (L/D), measured as sectional force in the midspan position. In figure 3, results for two Reynolds numbers have been plotted: (*a*) $Re = 1.6 \times 10^4$ and (*b*) 4.3×10^4. Curve (*b*) shows how the fluctuating lift increases as the end plate separation is decreased at the higher Reynolds number. The increase starts at separations smaller than 6–7 body diameters (D) and the fluctuating lift reaches a peak at $1D$ end plate separation. At aspect ratios below 1, the vortex shedding diminishes, probably owing to significant interference from the boundary layers on the plates. In contrast, for the lower Reynolds number, curve (*a*), aspect ratio effects are very weak. Only a slight increase in c_L' was obtained at reduced aspect ratio, but the decrease for aspect ratios smaller than 1 was observed for both Reynolds numbers. Figure 4 (*a–d*) shows how c_L' changes with increases in Reynolds number from 5.1×10^4 up to 1.3×10^5. At the two highest Reynolds numbers tested the flow enters a critical Reynolds number

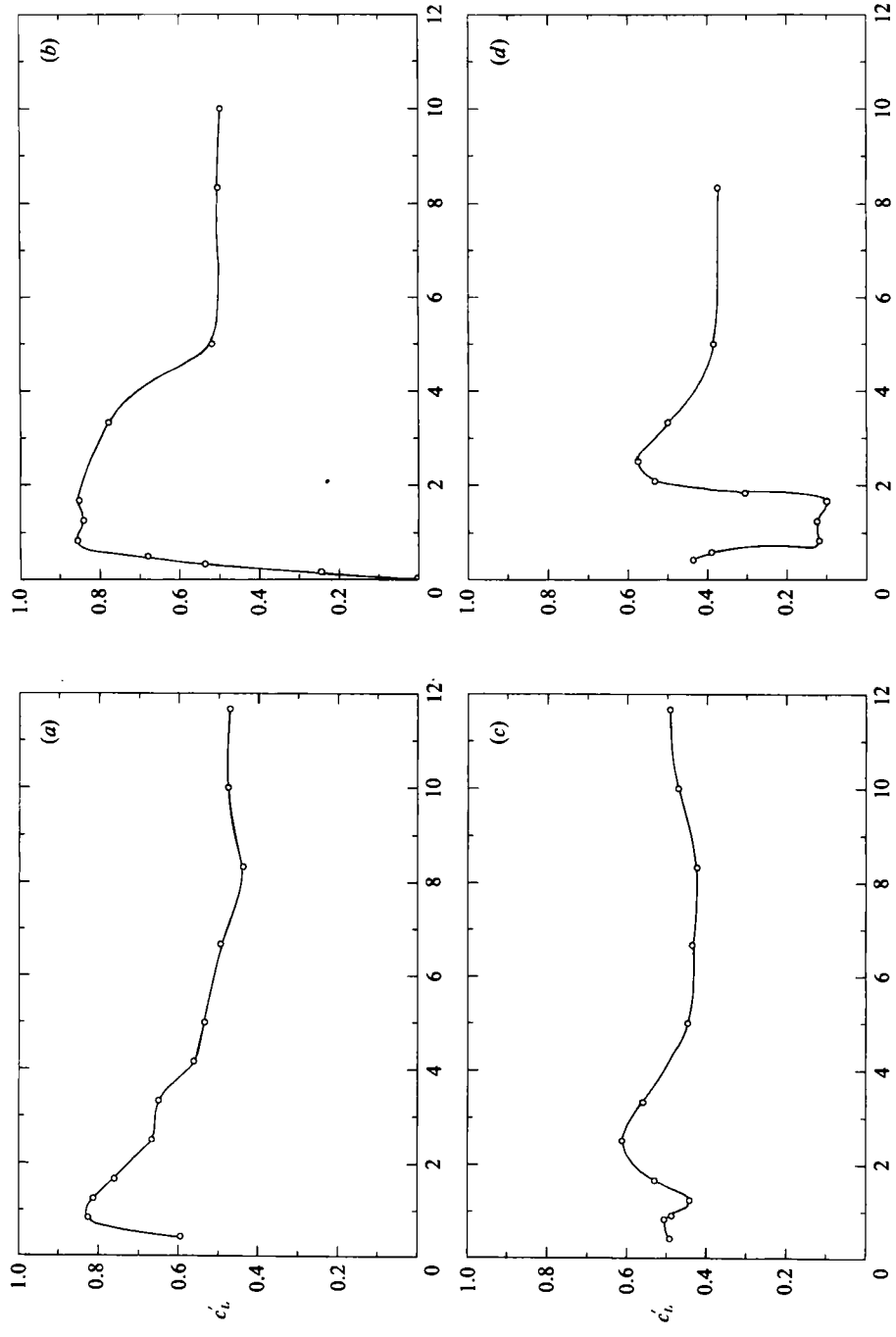

FIGURE 4. Fluctuating lift *vs.* end plate separation: (*a*) $Re = 5.1 \times 10^4$, (*b*) $Re = 7.1 \times 10^4$, (*c*) $Re = 1.2 \times 10^5$, (*d*) $Re = 1.3 \times 10^5$.

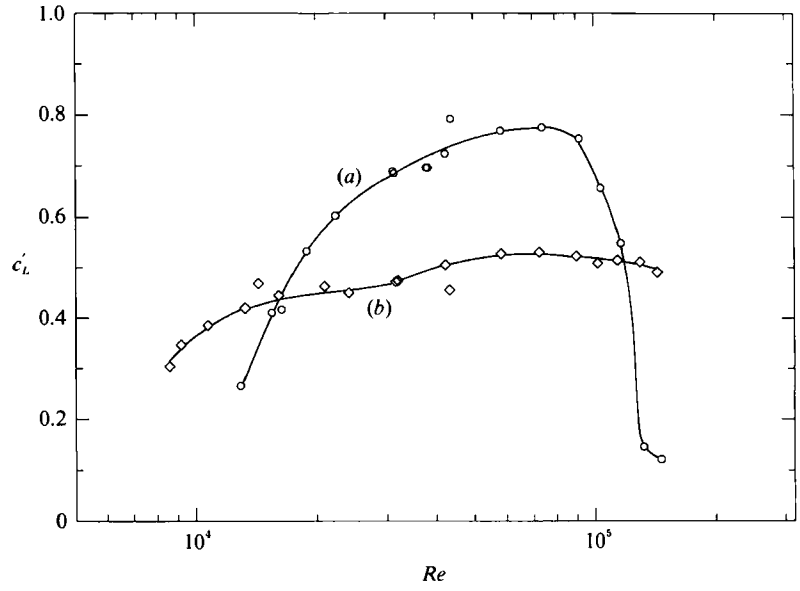

FIGURE 5. The fluctuating lift coefficient *vs.* Reynolds number for different aspect ratios: (*a*) $L/D = 1$, (*b*) $L/D = 6.7$.

range. For the two lower Reynolds numbers, i.e. 5.1×10^4 (figure 4*a*) and 7.0×10^4 (figure 4*b*), c'_L reaches a peak at end plate separations around $1D$, which is similar to the behaviour observed for $Re = 4.3 \times 10^4$. Increasing the Reynolds number further for small aspect ratios, the flow undergoes a transition into a regime with virtually no regular vortex shedding at all. Consequently, the fluctuating force diminishes sharply, as shown in figure 4(*d*). A reduction in c'_L at an aspect ratio of 1 is seen to be just appearing in figure 4(*c*) for $Re = 1.2 \times 10^5$. The trend of increasing fluctuating lift for narrow end plate separations is reversed for aspect ratios around 2.5. But at only a slightly increased Reynolds number ($Re = 1.3 \times 10^5$), the fluctuating lift is sharply reduced at aspect ratios of about 1. At low aspect ratios vortex shedding is suppressed but at end plate separations larger than about $2.5D$, the regular shedding pattern is re-established. Above $L/D = 6$, a constant value of c'_L of 0.4 is obtained. It was observed in the transitional range that the force signal does not exhibit a continuous reduction in magnitude with increasingly higher Reynolds numbers. Instead, for transitional small aspect ratios, the flow randomly alternates between strong regular vortex shedding and weak irregular shedding. On increasing the Reynolds number the latter mode becomes more dominant and thereby causes a dramatic reduction in the fluctuating forces.

3.2. *Coefficient of fluctuating lift vs. Reynolds number*

As described above the sectional life force coefficient was measured at several Reynolds numbers. In figure 5, c'_L obtained in the midspan position is plotted against Re. Two cases are considered here: $L/D = 1$ and 6.7, being representative for small and large aspect ratio flow respectively. For small aspect ratio there is a very strong Reynolds number dependence. The largest change in c'_L with aspect ratio at a constant Reynolds number was obtained at $Re = 4.2 \times 10^4$, where c'_L at $L/D = 0.8$ exceeds c'_L for $L/D = 10$ by 80%. Further, a sharp drop of c'_L at the onset of a critical Reynolds number range can be seen for the small aspect ratio case. The fall starts at

$Re = 6 \times 10^4$, but the lowest c'_L values following the complete suppression of strong regular vortex shedding appear only at $Re = 1{,}3 \times 10^5$. At the lower end of the Reynolds number range examined small aspect ratio also causes a reduction in c'_L, i.e. for Reynolds numbers smaller than 1.7×10^4 and down to the lower boundary of the measured Reynolds number range ($Re = 1.0 \times 10^4$). Whilst the small aspect ratio flow appears to be very Reynolds number dependent, there is only a small variation of c'_L with Reynolds number for $L/D = 6.7$.

4. Mean and fluctuating drag

In this section results are presented which demonstrate a correlation between the fluctuating lift and the mean drag. Figure 6 shows the change of the coefficient of sectional mean drag with reduced aspect ratio for two Reynolds numbers (4.3×10^4 and 1.3×10^5). The curve for the higher Reynolds number represents the range where, for small aspect ratios, an onset of a critical Reynolds number was observed. It can be seen that at large end plate separations ($5D$–$10D$), there is little effect of aspect ratio on $\overline{c_D}$ measured at the midspan position for these Reynolds numbers. Reducing the end plate separation below $4D$ causes an increase in the mean drag, which is thought to be related to vigorous vortex shedding associated with increased fluctuating lift. The maximum $\overline{c_D}$ achieved, for $Re = 4.3 \times 10^4$ and $L/D = 1$ was 1.47. Comparing the aspect ratio effect on $\overline{c_D}$ with its effect on fluctuating lift shows that for a given Reynolds number the two respond almost together. One can conclude that the more vigorous vortex shedding, with its associated stronger fluctuating lift reduces the base pressure and thereby increases the steady drag. Comparing fluctuation lift and steady drag coefficient results (figures 5 and 6), it is clear that the changes found in steady drag are substantially smaller than the changes in the fluctuating lift.

5. Pressure distribution around the cylinder

Returning to the vortex shedding breakdown for small aspect ratio at $Re = 1.3 \times 10^5$, the question arises whether this critical flow is connected with the traditional critical Reynolds number seen, for example, in the results in figure 20 of Schewe (1983) at $Re = 3 \times 10^5$. The latter critical flow is known to arise from transition in the free shear layers creeping up to the cylinder causing reattachment and secondary separation at 120° from the forward stagnation point. Figure 7 shows comparisons of pressure distribution of (*a*) critical flow caused by small aspect ratio at $Re = 1.3 \times 10^5$, (*b*) regular vortex shedding flow characterizing subcritical flow at larger aspect ratio, and (*c*) critical flow reported by Fage & Falkner (1931) at $Re = 2.1 \times 10^5$ and a large aspect ratio of 8. The figure shows that shedding breakdown at small aspect ratio features a similar type of separation as the subcritical case, since the pressure distributions show similar behaviour in the separation region, but the lack of regular vortex shedding decreases the base suction. Thus the pressure remains higher in case (*a*) than (*b*), resulting in a higher base pressure. Surface flow visualization carried out in cases (*a*) and (*b*) support this observation, where the separation point in both cases stayed near 80° from the forward stagnation point. Case (*c*) obtained from Fage & Falkner, on the other hand, is typical for critical flow caused by transition effects at $Re = 2$–3×10^5 resulting in a secondary separation near 120° from the forward stagnation point. Their aspect ratio of 8 should be considered as large in this context and is hence not the cause of vortex shedding

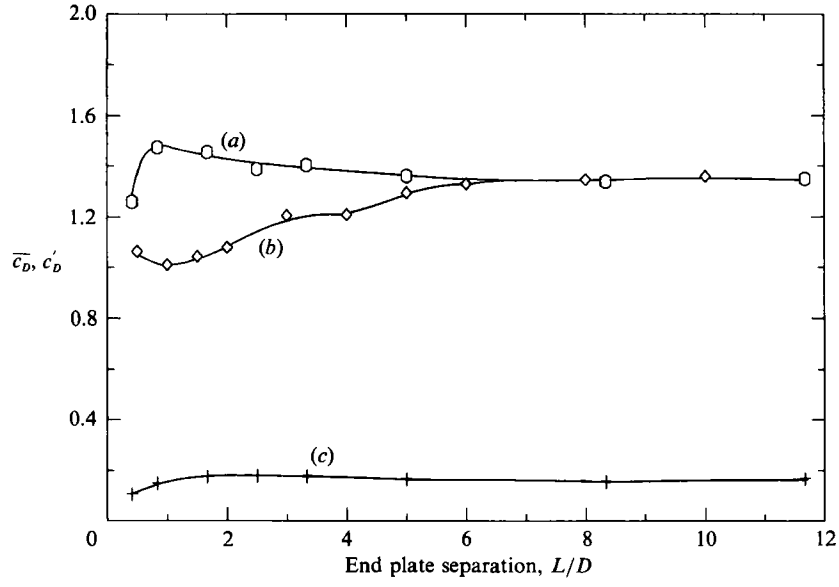

FIGURE 6. Mean drag coefficient: (*a*) $Re = 4.3 \times 10^4$, (*b*) $Re = 1.3 \times 10^5$. Fluctuating drag coefficients: (*c*) $Re = 4.3 \times 10^4$.

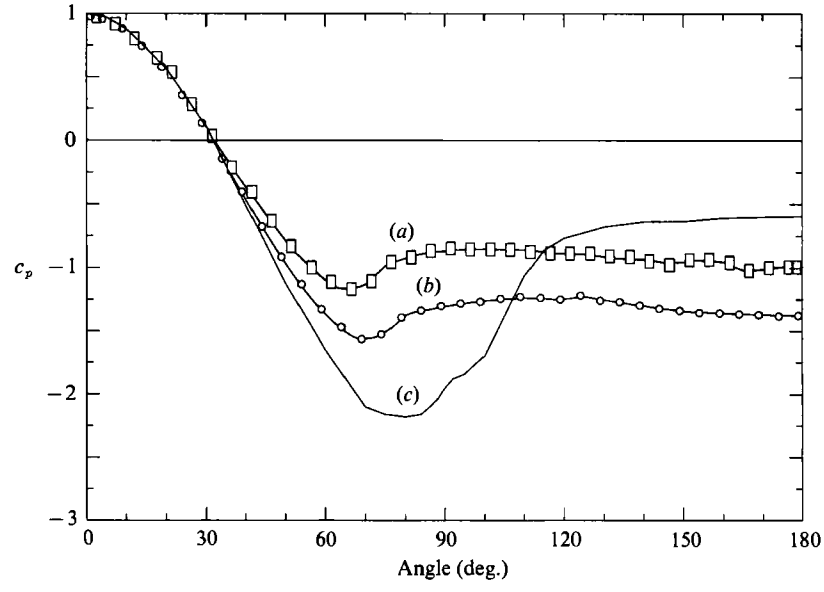

FIGURE 7. Pressure distribution around the cylinder at: (*a*) $Re = 1.3 \times 10^5$, $L/D = 1.25$; (*b*) $Re = 1.3 \times 10^5$, $L/D = 10$; (*c*) Fage & Falkner: $Re = 2.1 \times 10^5$, $L/D = 8.1$.

breakdown. Figure 8 shows a pressure distribution corresponding to the case of magnified vortex shedding forces at $Re = 4.0 \times 10^4$ and $L/D = 1$ compared with the weaker fluctuating lift force case at $L/D = 10$. These pressure distributions deviate significantly only after 150°, indicating that the laminar separation process is not affected by the magnification of the fluctuating wake pressure. Hence the local mean

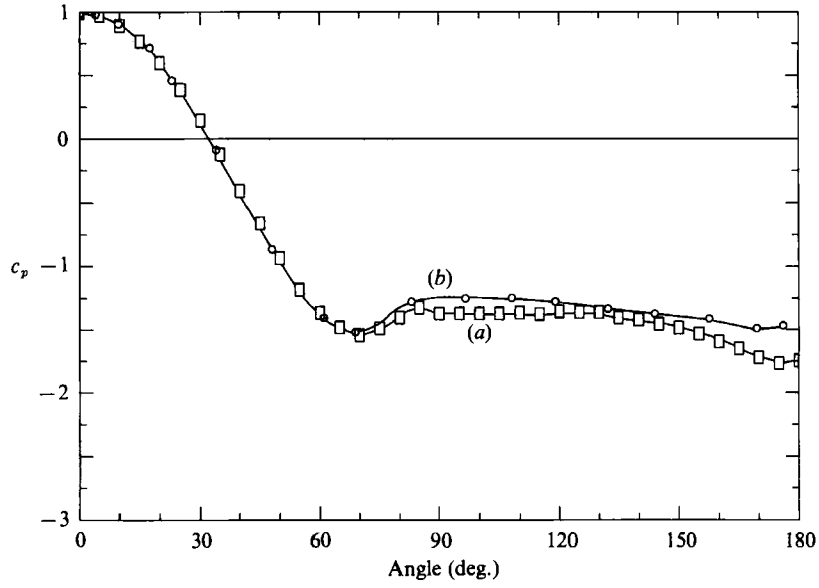

FIGURE 8. Pressure distribution around the cylinder at $Re = 4.0 \times 10^5$: (*a*) $L/D = 1$, (*b*) $L/D = 10$.

flow pattern around the cylinder seems to remain virtually unchanged, apart from the change in the base pressure.

6. Vortex formation length

The fluctuating velocity was recorded along the centreline of the cylinder wake. This measurement was performed to detect the distance (X_T/D) from the cylinder axis to the first peak in fluctuating velocity, as this is considered a good measure of where roll-up of the shear layer into a vortex takes place. In the highly unsteady flow region behind a cylinder a hot-wire does not provide a precise measurement of the velocity fluctuations. However, a number of researchers have taken the peak in fluctuating signal output to indicate the vortex formation position. The hot-wire probe was positioned with its axis parallel to the cylinder axis so as to be responsive to velocity components perpendicular to the cylinder axis. The vortex formation distance varies from one vortex to another and hence a large number of samples of the velocity are required to achieve converging mean-square values. In figure 9 four curves are plotted, for two Reynolds numbers at two different aspect ratios. At the lower Reynolds number ($Re = 1.3 \times 10^4$) very little effect of aspect ratio should be detected as figure 5 shows that this is a case close to a Reynolds number where c'_L is found to be insensitive to aspect ratio effects. Unexpectedly, a difference in formation length was found, with the peak values of indicated fluctuating velocity occurring at $1.5D$ and $1.35D$ for large and small aspect ratio respectively. However, each of these curves has a plateau rather than a sharp peak, especially the $L/D = 10$ case. These plateaux stretch from $X_T/D = 1.32$–1.51 for $L/D = 1$ and $X_T/D = 1.25$–1.63 for $L/D = 10$. When taking the middle position in each plateau better agreement is achieved, 1.42 compared with 1.44. The higher Reynolds number (4.2×10^4), where increased fluctuating lift was recorded, showed a decrease in formation length when the aspect ratio was reduced. The reduction is from $X_T/D =$

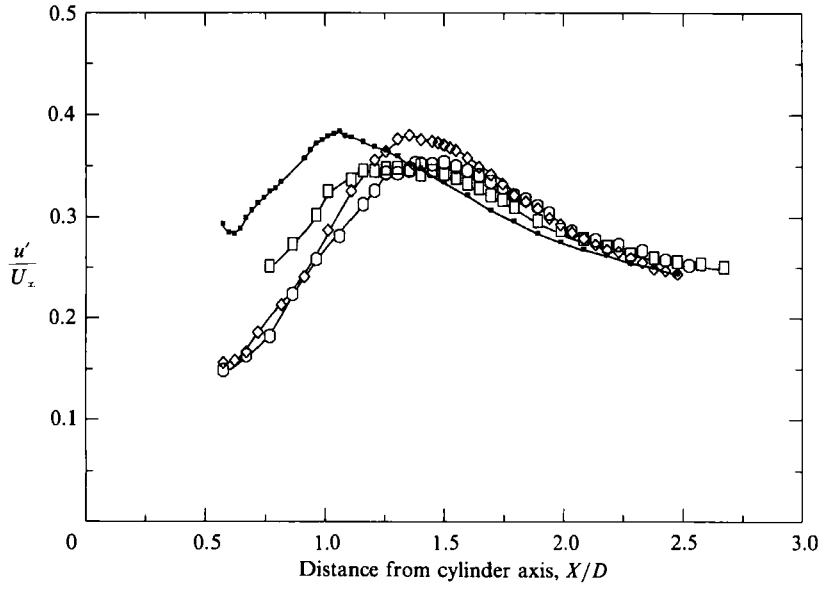

FIGURE 9. Fluctuating velocity along the wake centreline: (*a*) —■—, $L/D = 1$, $Re = 4.2 \times 10^4$; (*b*) —□—, $L/D = 10$, $Re = 4.2 \times 10^4$; (*c*) —◇—, $L/D = 1$, $Re = 1.3 \times 10^4$; (*d*) —○—, $L/D = 10$, $Re = 1.3 \times 10^4$.

1.30 to 1.06. Although the method used here for finding the vortex formation length is somewhat imprecise it is clear from figure 9 that the vortex formation length is significantly shorter for $L/D = 1$ and $Re = 4.2 \times 10^4$. Hence it can be concluded that the more vigorous vortex shedding, with its associated stronger fluctuating forces, is coupled with a definite decrease in the vortex formation length.

7. Shedding frequency analysis

The previous sections have shown that fluctuating lift, mean drag and vortex formation length are affected by changes in aspect ratio. It follows that the vortex shedding frequency may be affected since the wake parameters are interdependent. Spectral analysis was performed on the signal recorded by a hot wire positioned just outside the near-wake region. In figure 10, normalized power spectral density (PSD $\times U/u^2D$) is plotted against non-dimensional frequency (nD/U), where PSD is the power spectral density of the fluctuating velocity and u^2 is the mean square of the velocity. The small aspect ratio case (*a*) ($L/D = 1$) is compared with the large aspect ratio case (*b*) ($L/D = 11$) at $Re = 4.5 \times 10^4$. Curve (*a*) corresponds to a case of increased fluctuating lift (figure 3) and it can thus be seen that the Strouhal frequency is reduced. The Strouhal number in curve (*a*) is 0.17 compared with 0.19 in curve (*b*). Curve (*a*) shows a slight difference in the distribution of the power spectral density. In the low-frequency band ($nD/U < 0.1$) it exhibits lower spectral density. Instead, more of the energy in the signal is transferred to frequencies near the Strouhal frequency, where a larger peak spectral density was obtained (the peak occurring at $nD/U = 0.28$ is electrical noise of 50 Hz produced by the tunnel fan control system and should be disregarded). At lower Reynolds numbers one expects to find little or no effect of aspect ratio (as in figure 5 at $Re = 1.7 \times 10^4$), and it can be seen in figure 11 that this is indeed the case. These spectra were deduced from the

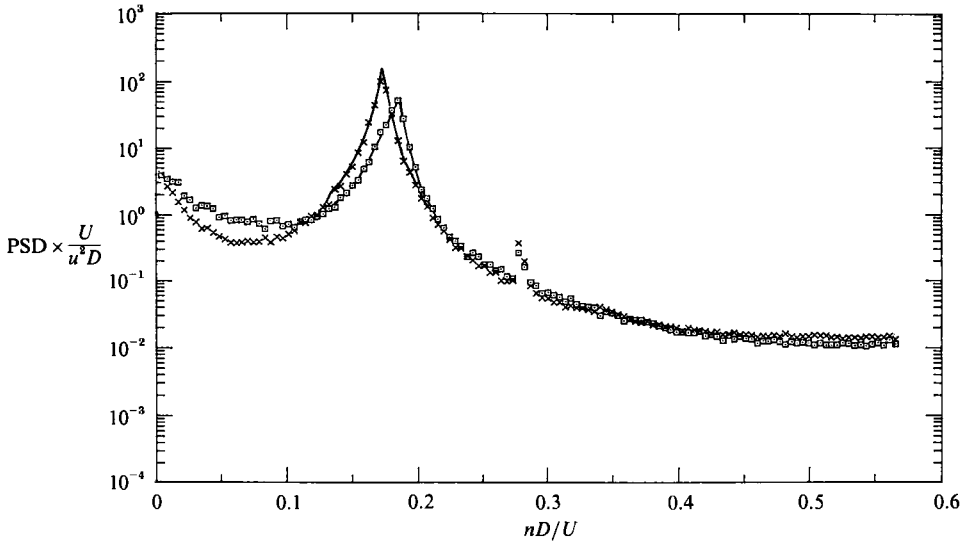

FIGURE 10. Frequency spectra for two different aspect ratios at $Re = 4.5 \times 10^4$: (*a*) ×, $L/D = 1$; (*b*) ⊡, $L/D = 6.7$.

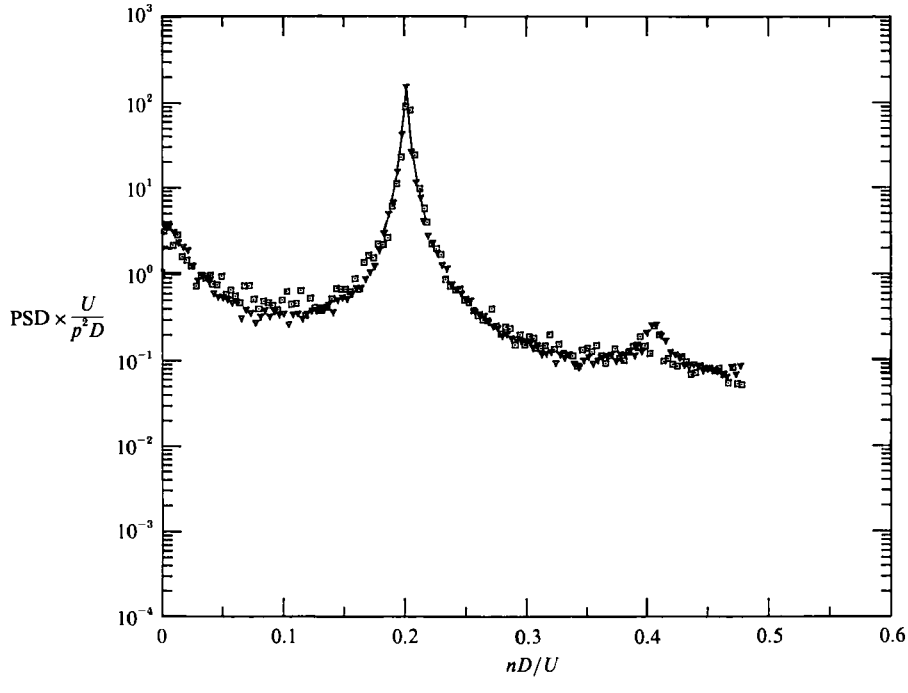

FIGURE 11. Frequency spectra for two different aspect ratios at $Re = 1.3 \times 10^4$: (*a*) ▼, $L/D = 1$; (*b*) ⊡, $L/D = 11$.

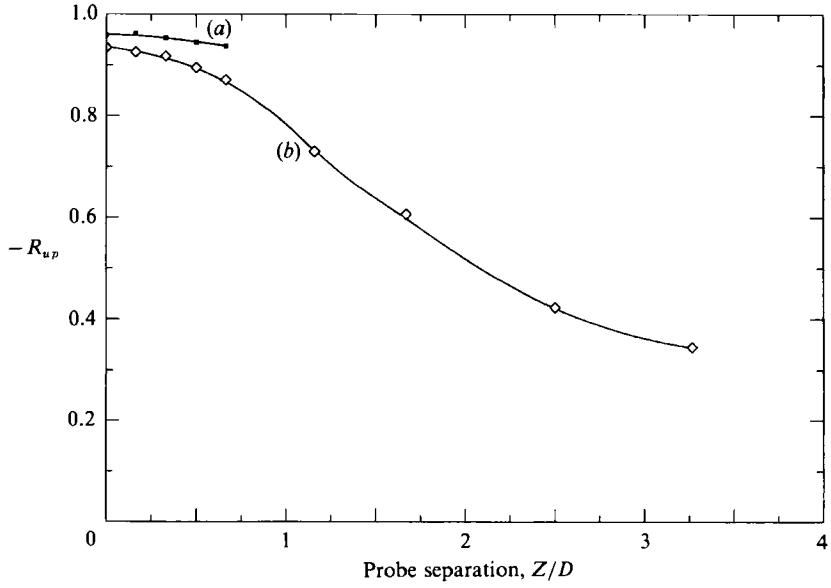

FIGURE 12. Cross-correlation of pressure and velocity (R_{up}) along the cylinder span, $Re = 5.1 \times 10^4$: (a) $L/D = 1.7$, (b) $L/D = 6.7$.

pressure signal recorded close to the hot-wire position. Two curves have been plotted at $Re = 1.3 \times 10^4$, (a) $L/D = 1$ and (b) $L/D = 11$, and the Strouhal number is 0.20 in both cases.

8. Spanwise correlation

In order to verify whether the enhancement of vortex shedding at small aspect ratio is connected with a more nearly two-dimensional flow, a spanwise two-point cross-correlation was measured. This was obtained as a correlation coefficient between pressure and velocity using a fixed pressure tap in the midspan position whilst traversing a hot-wire probe along the span at a distance $\frac{1}{3}D$ above the top of the cylinder. Both pressure tap or hot-wire probe were positioned at 90° from the forward stagnation point. In practice, the measured correlation coefficient always fell short of -1. This was because there was a phase lag between the pressure and velocity signals even with no spanwise separation between the hot wire and pressure tapping. Since pressure is to be used as phase reference the phase lag should not affect any conclusions to be drawn about the two-dimensionality of the flow. This phase lag was artificially compensated for by calculating the correlation coefficient as $\overline{u_p p_{i-n}}$ rather than $\overline{u_i p_i}$, where n is an integer constant representing a small time interval; the value of n was chosen so as to obtain the maximum possible correlation with the hot-wire positioned $\frac{1}{3}D$ above the pressure tapping. After this calibration, n was held constant whilst traversing the hot-wire probe along the span. Spanwise variations in the pressure and timing of the shed vortices became apparent as the separation of the hot wire and pressure tapping was increased. These latter variations are due to disturbances of the flow causing non-homogeneous rolled up vortex sheets along the cylinder span, and it is on these changes that we will focus our primary attention in the present study.

In figures 12 and 13 it can be seen how the spanwise correlation has increased for narrow end plate separations at $Re = 5.1 \times 10^4$ and 7.1×10^4. According to figure 5,

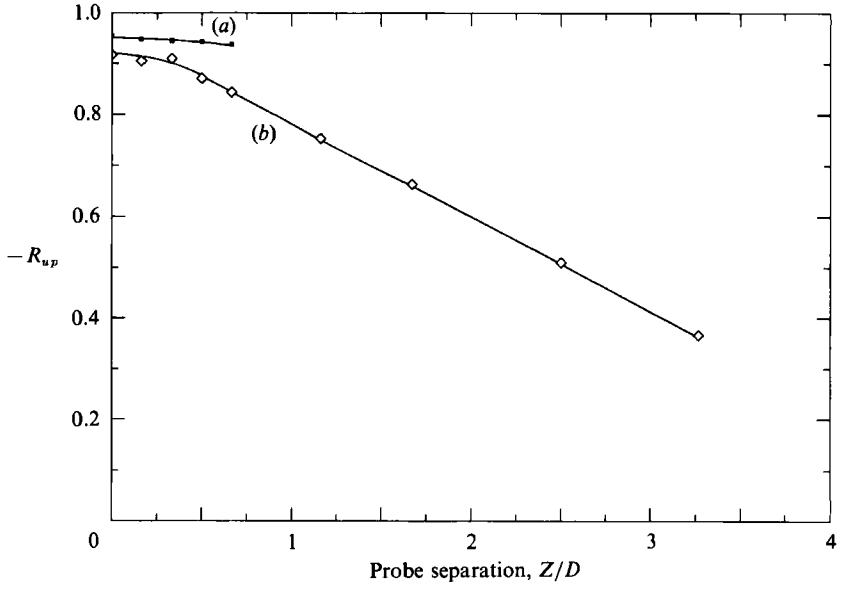

FIGURE 13. Cross-correlation of pressure and velocity (R_{up}) along the cylinder span. $Re = 7.1 \times 10^4$: (*a*) $L/D = 1.7$, (*b*) $L/D = 6.7$.

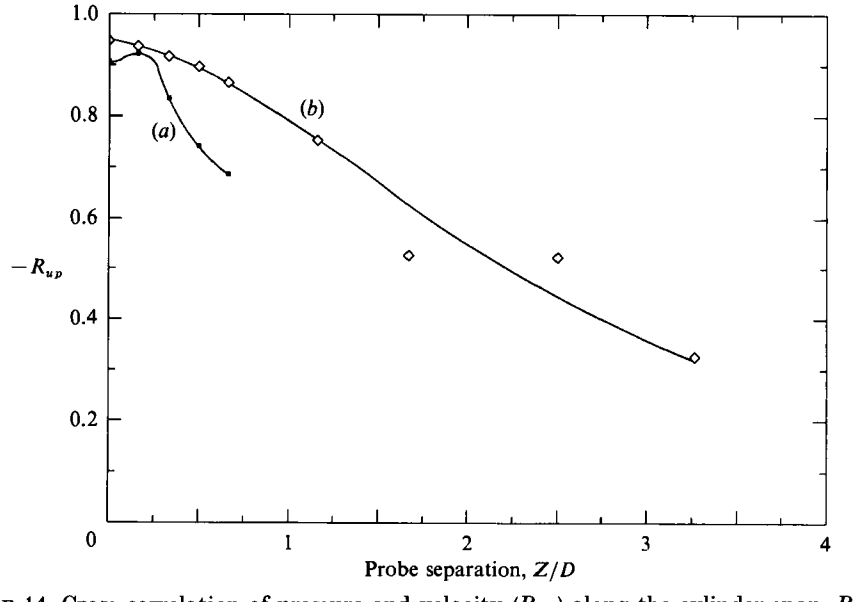

FIGURE 14. Cross-correlation of pressure and velocity (R_{up}) along the cylinder span. $Re = 1.3 \times 10^5$: (*a*) $L/D = 1.7$, (*b*) $L/D = 6.7$.

this is a case where reduced aspect ratio gives increased fluctuating lift. Thus it can be concluded that the flow with stronger vortex shedding also has enhanced spanwise correlation. The flow pattern features coupled with the changes in the correlation coefficient will be further examined in §10. Figure 14 shows that for a higher Reynolds number approaching the critical range, i.e. at $Re = 1.3 \times 10^5$, the case is reversed, with the small aspect ratio showing a sharp drop in correlation due to

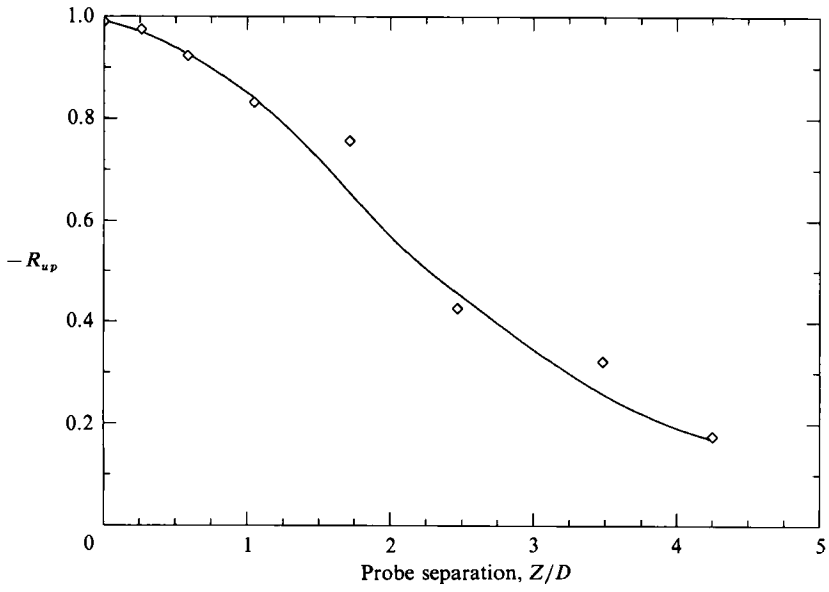

FIGURE 15. Cross-correlation of pressure and velocity (R_{up}) along the cylinder span. $Re = 5.7 \times 10^4$, $L/D = 10$.

disturbed vortex shedding whereas the large aspect ratio case behaves very much like that of the lower Reynolds numbers in figure 12 and 13. Figure 15 shows the decay of the spanwise correlation along the cylinder span at $Re = 5.7 \times 10^4$ and $L/D = 10$. A crude estimation of the correlation length is $2.5D$.

9. Spanwise variation of fluctuating lift

The experiments have shown that changing the aspect ratio, particularly at some Reynolds numbers, affects the mean and fluctuating forces, the shedding frequency and vortex formation length. So far, however, the force measurements presented have been obtained from the midspan position and accordingly give no information about the distribution along the span. At large end plate separations it is expected that there will be a region of non-uniform fluctuating lift in the vicinity of the end plate. If the span is long enough for the opposing side boundary effects not to interact, then the flow in the centre will be different from the boundary-affected zones and there may be differences in vortex strength and shedding frequency. For small aspect ratios the whole flow will be affected by the end boundaries. Figures 16 and 17 show the variation of the coefficient of fluctuating lift along one half of the cylinder span starting from the midspan position for two different Reynolds numbers. The end plate position has been marked in the figures by a vertical dotted line. In figure 16, for $Re = 4.3 \times 10^4$, it can be seen that curve (a) with $L/D = 1$ reaches a peak in the midspan position. Away from the centre c'_L decays but is reinforced near the end plate. The maximum fluctuating lift is reached $0.125D$ from the end plates. Curve (b) for $L/D = 4$, has the most uniform distribution of the three curves, but there is also a dip $0.25D$ from the end plate which again recovers to a higher c'_L value nearer the end plate. Curve (c) for $L/D = 6.7$ is the only case with a large enough end plate separation to ensure that the flow in the midspan position is likely to produce a value of c'_L unaffected by the end plates. Even so, it is only over

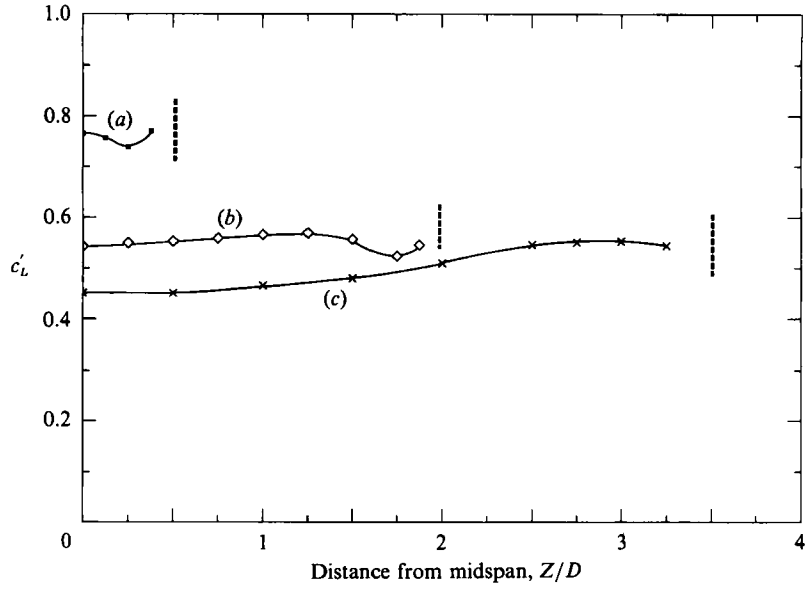

FIGURE 16. The fluctuating lift coefficient distribution along the cylinder span, $Re = 4.3 \times 10^4$: (*a*) $L/D = 1$, (*b*) $L/D = 4$, (*c*) $L/D = 6.7$.

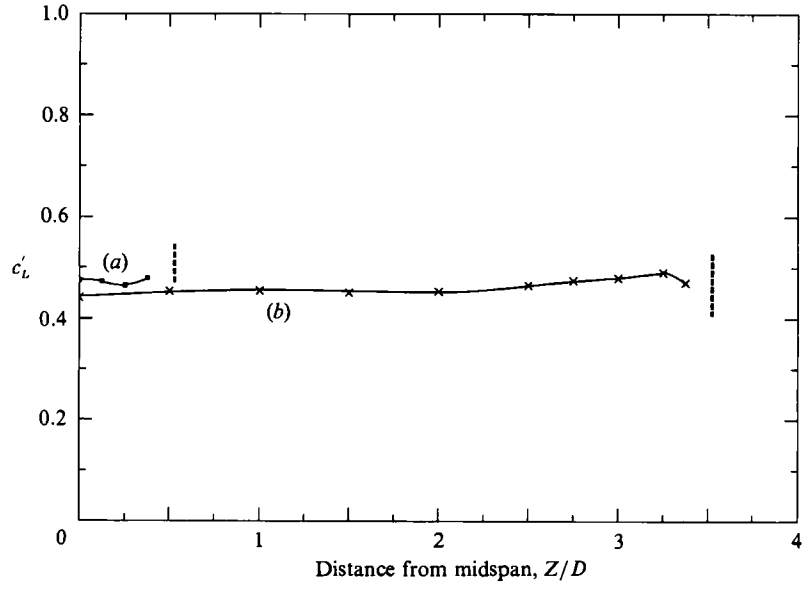

FIGURE 17. The fluctuating lift coefficient distribution along the cylinder span, $Re = 1.7 \times 10^4$: (*a*) $L/D = 1$, (*b*) $L/D = 6.7$.

a central length of about $1D$ that c'_L remains constant. Approaching an end plate, c'_L increases and reaches a maximum $0.5D$ away from the plate. Similar measurements were also performed for a lower Reynolds number where, according to figure 5, the fluctuating lift was rather insensitive to aspect ratio effects. Figure 17 shows the distribution at $Re = 1.7 \times 10^4$. As expected from the previous c'_L results there is only a small difference between the $1D$ and the $6.7D$ aspect ratio cases. The small

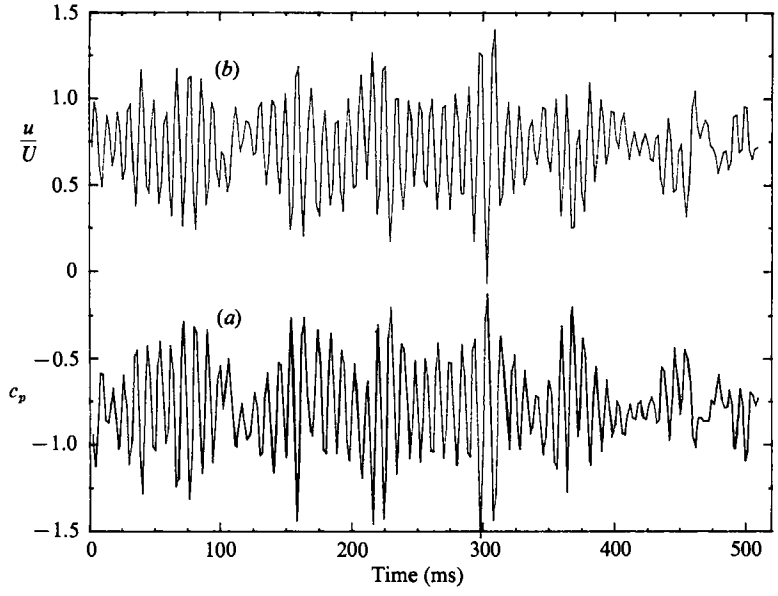

FIGURE 18. Signal traces of (*a*) pressure and (*b*) velocity at 90° from the forward stagnation point in the midspan position $\frac{1}{3}D$ above the pressure tap. $Re = 1.3 \times 10^5$, $L/D = 6.7$.

variations of c'_L along the span suggest that the vortex shedding strength does not change approaching the end plates at this Reynolds number, in contrast to the higher Reynolds number measurements.

10. Discussion

These experiments have shown that appropriate end plates, particularly at some Reynolds numbers make the vortex shedding and presumably the whole wake flow more nearly two-dimensional. So far the results shown here have been of time-averaged flow parameters. The spanwise variations in the flow can be more easily understood when signal traces are studied, such as those shown in figures 18 and 19. Figure 18 shows signal traces of pressure and velocity at two points, pressure (*a*) on the surface and velocity (*b*) $\frac{1}{3}D$ above the cylinder (90° from the forward stagnation point), both in the midspan position. In this case there is good correlation between the two signals ($R_{up} = -0.95$). Even the smallest disturbances appear simultaneously and are hence well correlated in both traces. Figure 19 shows a different picture: here the measurement points are separated by $2.5D$ along the cylinder span and the correlation has dropped to $R_{up} = -0.5$. From the analysis of many traces with the transducers at this separation, the weak shedding cycles that seem to appear at time intervals of 10–20 times the Strouhal period are not well correlated between the two signals. The frequency of events at the two stations appears almost constant but the phase lag can vary quite randomly. The origin of the apparently weakest shedding cycles is not clear, they may be due to disturbances to the triggering of the vortex shedding development. After a disturbance in the sinusoidal shedding pattern has appeared, the build-up of regular strong shedding takes a number of cycles to be re-established. If the initial onset of vortex shedding is repeatedly being disturbed, then the regular shedding can be weakened for a considerable proportion of the shedding cycles. Clearly this modulation of the pressure amplitude, which has not been

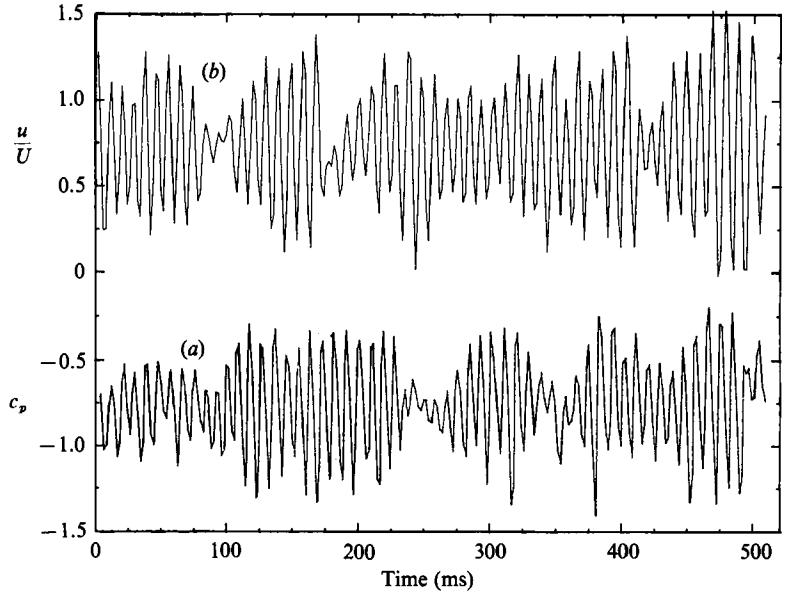

FIGURE 19. Signal traces of (*a*) pressure and (*b*) velocity at positions (*a*) (midspan) and (*b*) (offset from *a* by 2.5*D* along the span). $Re = 1.3 \times 10^5$, $L/D = 6.7$.

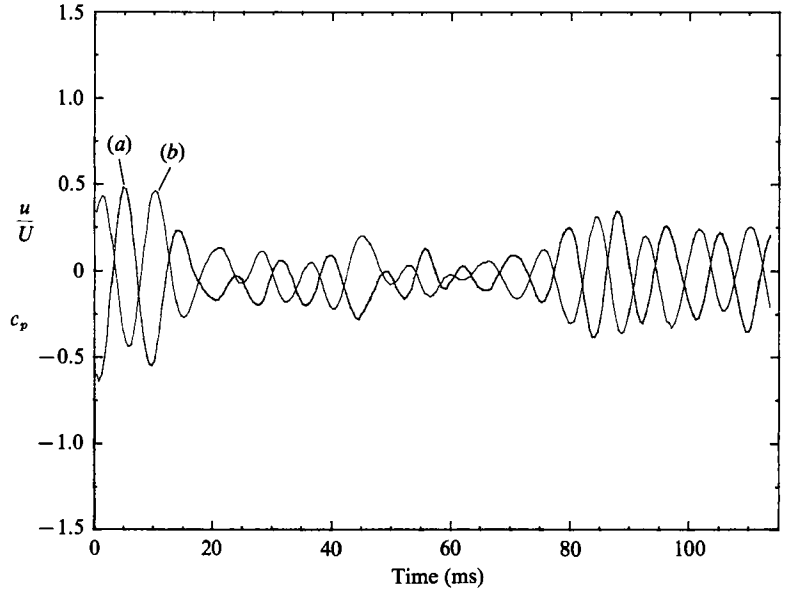

FIGURE 20. Signal traces (midspan position) of (*a*) pressure at 90° from the forward stagnation point and (*b*) velocity $\frac{1}{8}D$ above the pressure tap. $Re = 1.3 \times 10^5$, $L/D = 6.7$.

observed in two-dimensional numerical simulations, is contributing strongly to a lowering of the time-averaged fluctuating force. Moreover, as the shedding frequency does not remain constant while the pressure amplitude changes, it can be expected that this will lead to unsteady three-dimensional flow along the span. Presumably these small disturbances cannot be avoided in real flows where there is turbulence

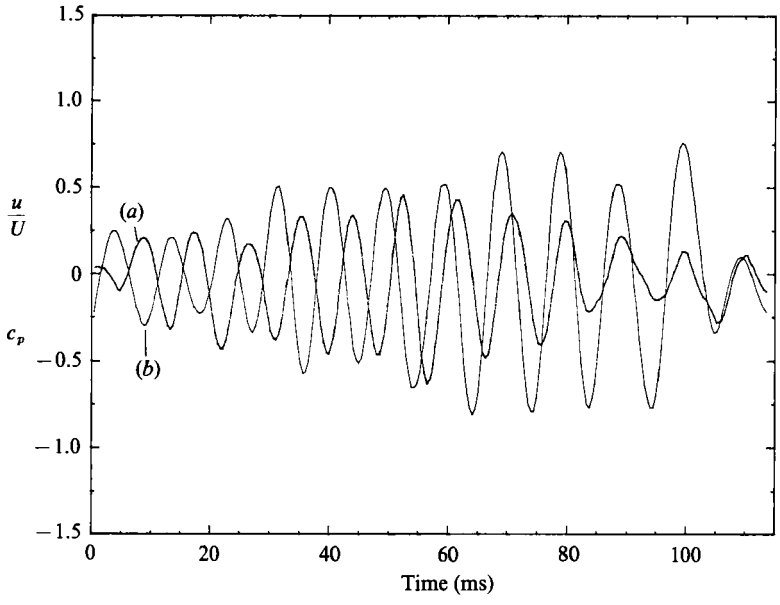

FIGURE 21. Signal traces of (*a*) pressure and (*b*) velocity (*b*) is offset from (*a*) (midspan) by a distance of 2.5*D*. $Re = 1.3 \times 10^5$, $L/D = 6.7$.

and wall boundary interference. A single disturbed vortex can therefore have quite a large influence on time-averaged parameters since full shedding strength will not be regained until perhaps the shedding is in phase over a substantial spanwise length. The disturbances that cause this modulation are presumably strongly dependent on end conditions and Reynolds number, according to experiments conducted in the range $Re = 1 \times 10^4 - 1.3 \times 10^5$. The weak shedding mode seems to reappear somewhat periodically at about 10–20 times the Strouhal period with a duration of about 3–7 shedding cycles. This behaviour is consistent with there being some form of unsteady spanwise cellular structure to the vortices.

The random phase shift between different spanwise positions can be seen even more clearly in figures 20 and 21, plotted on an expanded timescale. Figure 20 shows the case where the hot-wire probe is positioned directly above the pressure tap. It can be seen that the signal traces follow each other almost perfectly by 180° and there is no phase drifting between the signals (cross correlation $R_{up} = -0.95$). Figure 21, on the other hand, with the probes separated by 2.5*D* along the span, shows that the phase lag can shift quickly. In this case there is a phase change between the signals of 180° during the course of only seven periods. This phase shift occurs because the weak shedding cycles move to a higher frequency whilst the signal with stronger shedding (*b*) is constant close to the Strouhal frequency. The difference in dimensionless shedding frequency (nD/U) is about 0.03. It was also observed that very weak shedding cycles, i.e. with an amplitude less than about 0.1 c_p units, are predominantly disturbed and less sinusoidal causing the frequency to drift around the Strouhal frequency. Eventually there is also a chance of missing a vortex roll-up if it is too weak.

The presence of three-dimensional effects on circular cylinder flow may help to explain differences observed between experiments and predictions from two-dimensional numerical simulations. In figure 22, c'_L is plotted against Reynolds

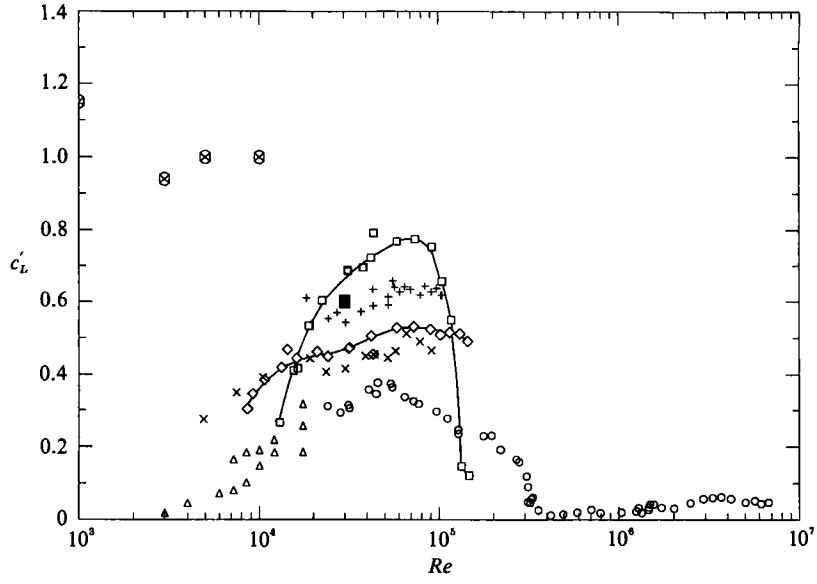

FIGURE 22. The fluctuating lift coefficient *vs.* Reynolds number for different aspect ratios limited by end plates (*a–d*) or end walls (*e,f*). Experiments: present; (*a*) —□—, $L/D = 1$; (*b*) —◇—, $L/D = 6.7$; (*c*) +, Keefe, $L/D = 3$; (*d*) ×, Keefe, $L/D = 18$, (*e*) ○, Schewe, $L/D = 10$; (*f*) △, Tadrist *et al.* Numerical simulations: ⊠, Braza *et al.*, two-dimensional direct simulation of Navier–Stokes equations; ■, Stansby, two-dimensional discrete vortex method.

number and shows a comparison between numerical results and the present experiments as well as some other experiments reported. Having established that there are appreciable three-dimensional effects in the flow, it is likely that different investigators will produce different results. It has been appreciated for a long time that there will be differences in c'_L depending on whether the force has been obtained from sectional pressure measurements or from a finite active length of the cylinder. The latter would produce an average of the force fluctuations along the active length and hence give a lower r.m.s. force value per span width than the r.m.s. force obtained from a very thin section of the span. The present results obtained for small aspect ratio ($L/D = 1$) show a very strong Reynolds number dependence, whereas for a larger aspect ratio of $L/D = 6.7$ there is very little variation with Reynolds number. Hence the strong Reynolds number dependence is only significant in combination with aspect ratio effects. In addition, the use of small aspect ratio caused an onset of a critical Reynolds number at $Re = 1.3 \times 10^5$, which was seen in figure 4(*d*). Other experimental results for a large and a small aspect ratio have been taken from the work reported by Keefe (1961) who used a short active force sensitive element. The active element itself had a spanwise length of 1*D*, and seems to produce results similar to the present sectional lift forces, with magnified fluctuating forces reported for reduced aspect ratio. Schewe's (1983) measurements give lower fluctuating lift values, which is to be expected, since his lift coefficients are based on force measurements using the entire cylinder length (10*D*) and will hence be affected by the limited spanwise correlation of vortex shedding. Tadrist *et al.* (1990) results are also obtained from the whole span ($12.5 < L/D < 30$). Their results using different cylinders, of which only samples are shown here, are somewhat scattered. However, the trend of sharply decreasing fluctuating lift on reducing the Reynolds number below 10^4 is evident.

In the region $1.7 \times 10^4 < Re < 1.0 \times 10^5$, experiments conducted at small aspect ratio gave increased fluctuating lift, where according to the measurements of spanwise correlation, the flow becomes more two-dimensional. The use of small aspect ratio seems to bring the experimentally obtained c'_L closer to the numerical ones obtained using a two-dimensional model. Stansby (1981) used a discrete vortex model to simulate a Reynolds number of 3×10^4. The c'_L value he obtained appears between our small aspect ratio (1) and large aspect ratio (6.7) value, which may not be surprising as his method is using some experimental input (separation positions and an empiric relation between mean rate of shedding of vorticity and free-stream velocity) from large aspect ratio cases which are then implemented in a two-dimensional computational scheme. The numerical results plotted in the lower Reynolds number range were reported by Braza *et al.* (1986, 1990), obtained from direct simulation of the Navier–Stokes equations in two dimensions. A comparison between the numerical and experimentally determined c'_L results show large deviations. The deviation between Stansby's result and the present at $Re = 3 \times 10^4$ may be expected but it is striking to see such a large deviation between the disturbance-free numerical direct simulation as in Braza *et al.* at $Re = 1.0 \times 10^4$ and experiments. Unfortunately Braza *et al.*'s results only overlap with the present measurements over a very small Reynolds number range. The use of small aspect ratio in the experiments, at least with the present end plates, does not reinforce the vortex shedding strength or make the flow more nearly two-dimensional in the Reynolds number range around $Re = 10^4$, and hence it is unlikely that the discrepancy between Braza *et al.*'s results and the present ones can be attributed to aspect ratio effects alone. It should be remembered, of course, that in the simulations only two-dimensional Reynolds stresses are developed.

The sharp decay of c'_L below $Re = 1.7 \times 10^4$ at $L/D = 1$ in the experiments is not fully understood and not yet fully investigated. In this Reynolds number range, large aspect ratio studies have previously established that the cylinder vortex shedding has an appreciable Reynolds number dependence. Also, we know that a bluff body placed on a plate can form horseshoe vortices developed from boundary-layer interactions on the plate and the cylinder foot. The interaction between this horseshoe vortex system and the cylinder vortex shedding has not been fully investigated. Studies focusing on details of these horseshoe vortices, but not primarily on the interaction with cylinder vortex shedding, have been carried out for example by Baker (1980), Bêlik (1973) and Dargahi (1989). Horseshoe vortices appear both for laminar and turbulent boundary layers but show increased complexity and a less regular structure with increased Reynolds number. Whether it is intrinsic cylinder vortex shedding features or the horseshoe vortex layer that is responsible for the additional Reynolds number sensitivity at small aspect ratios, remains to be clarified. Further, it was assessed by surface flow visualisation that no flow separation took place at the leading edge of the end plate, hence disturbances originating from separation bubbles upstream of the cylinder could be excluded.

11. Conclusions

Fluctuating forces on a circular cylinder in crossflow were measured for various aspect ratios by using moveable end plates. The end plates were designed according to a previous survey by Stansby (1974) aimed at optimizing end plate size. The Reynolds number range of the measurements stretched over the subcritical range ($8 \times 10^3 < Re < 1.4 \times 10^5$). The influence of aspect ratio (0.25–12) was recorded and

was found to have a most striking effect on the fluctuating lift. However, the effect of changing aspect ratio was found to be dependent very strongly on the Reynolds number. An increase in c'_L of 80% at small aspect ratio ($L/D = 0.8$) was measured at $Re = 4.2 \times 10^4$, whilst a decrease of c'_L was obtained for $Re < 1.7 \times 10^4$. At this lower boundary of the measured Reynolds number range, it was found that aspect ratio produced only a very weak effect on the flow. At the upper boundary of the Reynolds number range a different pattern was observed, with regular vortex shedding disappearing for very small aspect ratios (1–3), but with a subcritical type of separation at 80° from the forward stagnation point.

Simultaneously with the changes in fluctuating lift, the shedding frequency altered. A lower shedding frequency was found to be associated with increased fluctuating lift. The largest change in Strouhl number recorded was from $S = 0.19$ ($Re = 4.5 \times 10^4$, $L/D = 6.7$) to $S = 0.17$ ($Re = 4.5 \times 10^4$, $L/D = 1$), measured in the midspan position. The strong magnification of the fluctuating lift that occurred at small end plate separations is believed to be linked to suppression of crossflows by the end plates. Measurements of spanwise correlation showed, for a case with increased fluctuating lift, that the spanwise correlation was indeed increased, bringing larger portions of the flow in phase along the span.

The fluctuating pressure on the cylinder at the 90° position from the forward stagnation point shows strong modulation which increased with Reynolds number, being significant at $Re = 2 \times 10^4$ and eventually becoming a dominating feature at $Re = 9 \times 10^4$. The irregularity in vortex shedding strength gives rise to a burst-like appearance of the signal trace. It was also found that with small aspect ratio not only did the fluctuating lift increase but also the vortex shedding took place with smaller amplitude modulation. Thus, at some Reynolds numbers (2.0×10^4–1.0×10^5), the use of appropriate end plates and small aspect ratio can give a more two-dimensional flow, which then results in an increase in both the fluctuating lift and mean drag. However, at the lowest Reynolds numbers measured (around $Re = 10^4$), aspect ratio causes either no effect or a weak reduction in c'_L for decreasing aspect ratio.

REFERENCES

Allen, H. J. & Vincenti, W. G. 1944 Wall interference in a two-dimensional-flow wind tunnel, with consideration of the effect of compressibility, *NACA Rep.* 782.

Baban, F., So, R. M. C. & Ötügen, M. V. 1989 Unsteady forces on circular cylinders in cross flow, *Exp. Fluids* **7**, 293–302.

Baker, C. J. 1979 The laminar horseshoe vortex. *J. Fluid Mech.* **95**, 347–367.

Baker, C. J. 1980 The turbulent horseshoe vortex. *J. Wind Engng Indust. Aerodyn.*, **6**, 9–23.

Bearman, P. W. 1965 Investigation of the flow behind a two-dimensional model with a blunt trailing edge and fitted with splitter plates. *J. Fluid Mech.* **21**, 241–256.

Bêlik, L. 1973 The secondary flow about circular cylinders mounted normal to a flat plate. *Aeronaut. Q.* **24**, 47–54.

Braza, M., Chassaing, P. & Ha Minh, H. 1986 Numerical study and physical analysis of the pressure and velocity fields in the near wake of a circular cylinder. *J. Fluid Mech.* **165**, 79–130.

Braza, M., Chassaing, P. & Ha Minh, H. 1990 Prediction of large-scale features in the wake of a circular cylinder. *Phys. Fluids* A **2**, 1461–1471.

Cowdrey, C. F. 1962 A note on the use of end plates to prevent three dimensional flow at the ends of bluff bodies. *NPL Aero Rep.* 1025.

Dargahi, B. 1989 The turbulent flow around a circular cylinder. *Exp. Fluids* **8**, 1–2.

Eisenlohr, H. & Eckelmann, H. 1989 Vortex splitting and its consequences in the vortex street wake of cylinders at low Reynolds number. *Phys. Fluids* A 1, 189–192.

FAGE, & FALKNER 1931 *Aero. Res. Counc. RM* 1369 (also in Goldstein, S. *Modern Developments in Fluid Dynamics*, vol. II, pp. 421–423. Oxford University Press, 1938).

FARIVAR, D. 1981 Turbulent flow around cylinders of finite length. *AIAA J.* **19**, 275–281.

GERICH, D. 1986 Über die Veränderung der Kármánschen Wirbelstraße durch Endscheiben an einem Kreiszylinder. *Mitteilungen* 81. *Max-Planck-Institut für Strömungsforschung*, ISSN 0374–1257 (in German).

GERICH, D. & ECKELMANN, H. 1982 Influence of end plates and free ends on the shedding frequency of circular cylinders. *J. Fluid Mech.* **122**, 109–121.

GERRARD, J. H. 1966 The mechanics of the formation region of vortices behind bluff bodies. *J. Fluid Mech.* **25**, 401–413.

HUMPHREYS, J. S. 1966 On a circular cylinder in a steady wind at transition Reynolds numbers. *J. Fluid Mech.* **9**, 603–612.

KACKER, S. C., PENNINGTON, B. & HILL, R. S. 1974 Fluctuating lift coefficient for a circular cylinder in crossflow. *J. Mech. Sci.* **16**, no. 4.

KAREEM, A., CHENG, C. M. & LU, P. C. 1989 Pressure and force fluctuations on isolated circular cylinders of finite height in boundary layer flows. *J. Fluids Struct.* **3**, 481–508.

KEEFE, R. T. 1961 An investigation of the fluctuating forces acting on a stationary circular cylinder in a subsonic stream of the associated soundfield. *University of Toronto, Institute of Aerophysics, Rep.* 76.

KÖNIG, M., EISENLOHR, H. & ECKELMANN, H. 1990 The fine structure in the Stroughal–Reynolds number relationship of the laminar wake of a circular cylinder. *Phys. Fluids* A **2**, 1607–1614.

KUBO, Y., MIYAZAKI, M., KATO, K. 1989 Effects of end plates and blockage of structural members on drag forces. *J. Wind Engng Indust. Aerodyn.* **32**, 329–342.

NISHIOKA, M. & SATO, H. 1974 Measurements of velocity distributions in the wake of a circular cylinder at low Reynolds numbers. *J. Fluid Mech.* **65**, 97–112.

RAMBERG, S. E. 1983 The effects of yaw and finite length upon the vortex wakes of stationary and vibrating circular cylinders. *J. Fluid Mech.* **123**, 81–107.

RICHTER, A. & NAUDASCHER, E. 1976 Fluctuating forces on a rigid circular cylinder in confined flow. *J. Fluid Mech.* **78**, 561–576.

ROSHKO, A. 1953 On the development of turbulent wakes from vortex streets. *NACA Rep.* 1191.

SCHEWE, G. 1983 On the force fluctuations acting on a circular cylinder in cross flow from subcritical up to transcritical Reynolds numbers. *J. Fluid Mech.* **133**, 265–285.

SIN, X. & SO, X. 1987 Local force measurements on finite span cylinders in a cross flow. *Trans. ASME* I: *J. Fluids Engng* **109**, 136–143.

SHAIR, F. H., GROVE, A. S., PETERSON, E. E. & ACRIVOS, A. 1965 The effect of confining walls on a steady wake behind a circular cylinder. *J. Fluid Mech.* **17**, 546–550.

SLAOUTI, A. & GERRARD, J. H. 1981 An experimental investigation of the end effects on the wake of a circular cylinder towed through water at low Reynolds numbers. *J. Fluid Mech.* **112**, 297–314.

STANSBY, P. K. 1974 The effect of end plates on the base pressure coefficient of a circular cylinder. *R. Aeronaut. J.* **78**, 36–37.

STANSBY, P. K. 1981 A numerical study of vortex shedding from one and two circular cylinders. *Aeronaut. Q.* 48–64.

SURRY, D. & STATHOPOULOS, T. 1977/8 An experimental approach to the economical measurements of spatially averaged wind loads. *J. Indust. Aerodyn.* **2**, 385–397.

SZEPESSY, S. 1988 End wall interaction and aspect ratio effect on vortex shedding and fluctuating forces on a circular cylinder. Research thesis, Chalmers University of Technology, ISSN 02809265.

TADRIST, H., MARTIN, R., TADRIST, L. & SEGUIN, P. 1990 Experimental investigation of fluctuating forces exerted on a cylindrical tube (Reynolds number from 3000 to 30000). *Phys. Fluids* A **2**, 12.

TANIDA, Y., OKAJIMA, A. & WATANABE Y. 1973 Stability of a circular cylinder oscillating in uniform flow or in a wake. *J. Fluid Mech.* **61**, 769–785.

WIESELBERGER, C. 1923 Ergebnisse der Aerodynamnischen Versuchsanstalt zu Göttingen. *Ann. Rep., Göttingen University* (in German).

WILLIAMSON, C. H. K. 1988*a* Defining a universal and continuous Strouhal–Reynolds number relationship for the laminar vortex shedding of a circular cylinder. *Phys. Fluids* **31**, 2742.

WILLIAMSON, C. H. K. 1988*b* The existence of two stages in the transition to three dimensionality of a cylinder wake. *Phys. Fluids* **31**, 3165.

WILLIAMSON, C. H. K. 1989 Oblique and parallel modes of vortex shedding in the wake of a circular cylinder at low Reynolds numbers. *J. Fluid Mech.* **206**, 579–627.

WILLIAMSON, C. H. K. & ROSHKO, A. 1990 Measurements of base pressure in the wake of a cylinder at low Reynolds numbers. *Z. Flugwiss. Weltraumforsch.* **14**, 38–46.

WEST, G. S. & APELT, C. J. 1982 The effects of tunnel blockage and aspect ratio on the mean flow past a circular cylinder with Reynolds number between 10^4 and 10^5. *J. Fluid Mech.* **114**, 361–377.

ZDRAVKOVICH, M. M., BRAND, V. P., MATTHEW, G. & WESTON, A. 1989 Flow past short circular cylinders with two free ends. *J. Fluid Mech.* **203**, 557–575.